

Surface exfoliation analysis on single-crystal silicon under compressed plasma flow action

J. Shen^{1,2,3}, I. Shahid¹, X. Yu^{1,4}, J. Zhang¹, H.W. Zhong¹, X. Yu¹, W.Y. Huang¹, G.Y. Liang¹, X.J. Cui¹, S. Yan⁵, X.F. Zhang¹ and X.Y. Le^{1,2,3}

Research Article

Cite this article: Shen J *et al.* (2018). Surface exfoliation analysis on single-crystal silicon under compressed plasma flow action. *Laser and Particle Beams* **36**, 129–135. <https://doi.org/10.1017/S026303461800006X>

Received: 7 December 2017

Accepted: 15 February 2018

Key words:

Compressed plasma flow; finite element method; fracture mechanics; J integral; single-crystal silicon

Author for correspondence:

X.Y. LE, School of Physics and Nuclear Energy Engineering, Beihang University, Beijing 100191, China. E-mail: xyle@buaa.edu.cn

¹School of Physics and Nuclear Energy Engineering, Beihang University, Beijing 100191, China; ²International Research Center for Nuclei and Particles in Cosmos, Beihang University, Beijing 100191, P.R. China; ³Beijing Key Laboratory of Advanced Nuclear Energy Materials and Physics, Beihang University, Beijing 100191, China; ⁴Tomsk Polytechnic University, Tomsk 634050, Russia and ⁵Institute of Heavy Ion Physics, Peking University, Beijing 100871, P.R. China

Abstract

Surface exfoliation was observed on single-crystal silicon surface under the action of compressed plasma flow (CPF). This phenomenon is mainly attributed to the strong transient thermal stress impact induced by CPF. To gain a better understanding of the mechanism, a micro scale model combined with thermal conduction and linear elastic fracture mechanics was built to analyze the thermal stress distribution after energy deposition. After computation with finite element method, J integral parameter was applied as the criterion for fracture initiation evaluation. It was demonstrated that the formation of surface exfoliation calls for specific material, crack depth, and CPF parameter. The results are potentially valuable for plasma/matter interaction understanding and CPF parameter optimization.

Introduction

During past decades, compressed plasma flow (CPF) was intensively studied as a typical source of intense thermal loads. Due to its thermal effect on the material surface, cracks, melting, ripples, droplets, evaporation, sublimation, or ablation will be formed. Similar burst of particles exists in the edge localized modes (ELMs) of the International Thermonuclear Experimental Reactor (ITER) as well, which is attributed to the turbulent transport process and plasma instability localized in the Tokamak edge region. Therefore, CPF is widely applied in material surface modification (Astashynski *et al.*, 2004) and environment simulation for ELMs (Garkusha *et al.*, 2014).

As one of the key ITER plasma-materials interaction issues (Federici *et al.*, 2003), material surface behavior under plasma thermal loads during type I ELMs was focused on plenty of works (Uglov *et al.* 2002, 2010; Astashynski *et al.* 2006; Dojčinović *et al.* 2010). Among these works, a quasi-stationary plasma gun of magnetoplasma compressor (MPC) was selected as the source of CPF. Filled with hydrogen at 100–5000 Pa, MPC working with initial capacitor banks voltage at 3–4 kV, inter-electrode voltage at 1.25 kV can generate CPF with current 80–100 kA, effective discharge duration 70 μ s, average plasma density $5 \times 10^{16} \text{ cm}^{-3}$, plasma flow velocity up to 120 km/s (Dojčinović *et al.*, 2007a; Dojčinović *et al.*, 2010).

After the action of CPF on (100) single-crystal silicon, two kinds of fracture are observed on the surface. One is surface-latticed linear fracture and the other is interlaminar planar fracture along {100} planes parallel to the surface (Dojčinović *et al.*, 2010). As shown in Figure 1, the latter fracture drives the occurrence of exfoliation, thus the surface fragment is removed and subsurface is revealed after exfoliation. As an indispensable part of the surface erosion, ablation and target mass losses, it is of great importance to study the formation mechanism of the interlaminar planar fracture for the investigation of plasma interaction with fusion reactor first wall materials.

To explain this, Griffith criterion has been used qualitatively (Dojčinović *et al.*, 2010), and the shock-wave theory was applied as well (Uglov *et al.*, 2010). Nevertheless, shock wave will not always result in fracture, and the role CPF played as a surface thermal load in the initiation of interlaminar fracture remains uncertain. For example, the reason why fracture features were only observed in the central part of the target (Dojčinović *et al.*, 2007b), and the reason why exfoliated layer was no more than 10 μ m are still to be shed light on.

Similarly, interlaminar fractures have also been discovered on the surface of silicon (Kovivchak *et al.*, 2012; Shen *et al.*, 2015) and tungsten (Remnev *et al.*, 2014) irradiated by another impact thermal load source intense pulsed ion beam (IPIB) (Zhao *et al.*, 2000). Even though different crystallographic orientation samples were utilized, interlaminar planar fracture parallel to the surface can always be observed. It was concluded that the non-uniformity of stress distribution between the bulk and outmost layer actuates the interlaminar

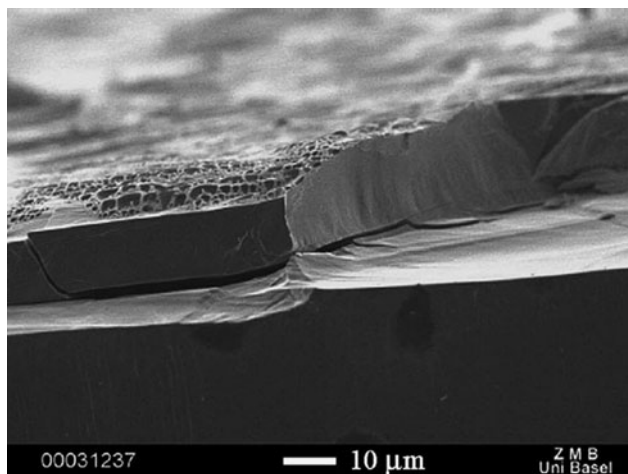


Fig. 1. SEM micrograph of cross-section of silicon (100) sample treated by CPF (Dojčinović *et al.*, 2010).

fracture parallel to the surface and finally leads to exfoliation. The J integral model combined with linear elastic mechanics has been applied to study the material behavior and judge the possibility of interlaminar planar fracture initiation (Shen *et al.*, 2017). It provides a good reference for the study of CPF, but considering the significantly different loading rates, energy deposition depths and energy density, it will be beneficial to develop a model specifically for CPF.

Taking (100) single-crystal silicon used in the experiment work (Dojčinović *et al.*, 2010) as an example, the purpose of this work is to better understand the formation mechanism of exfoliation driven by {100} interlaminar planar fracture under the action of CPF and reveal the answers for the above-mentioned problems. In this case, a quantitative relationship between CPF parameters and interlaminar fracture features should be constructed as well. It will eventually enable one to avoid these undesirable microstructures by adjusting CPF parameters, and in engineering applications, it can also be beneficial for the evaluation of surface behavior under different pulsed thermal loads.

Finite element method simulation

Before the model establishment, it is of great necessity to review the exfoliation process. At the very beginning, CPF action can lead to interlaminar planar fracture initiation along {100} planes parallel to the surface, and separate the outmost layer from the substrate surface. In this stage, even though {111} and {110} planes are usually more preferred at regular thermal stress loading (Danilewsky *et al.*, 2013), the CPF energy deposition with an energy density up to 1.0 MJ/m² during tens of microseconds is so strong and fast that the crystal directions with 0.5 J/m² maximum surface energy difference (Tanaka *et al.*, 2006) are too weak to make difference in this non-equilibrium state process. After crack growth, the surface energy is weakened rapidly and the binding energy difference becomes significant; thus, the cleavage fracture along {111} planes toward the surface occurs as demonstrated in the experiment (Dojčinović *et al.*, 2010). In this way, the exfoliated area is limited and bounded by cleavage fractures.

Based on the above process, it is important to firstly define the thermal load applied onto the study object for fracture mechanics

analysis. Afterwards, the main idea is to get the stress distribution around the notch, crack tip or some other crack sources within a specific area, and then use an appropriate criterion to evaluate the possibility of crack growth. Therefore, the processes of this work can be briefly illustrated in Figure 2.

According to the dimension of the silicon target used in (Dojčinović *et al.*, 2010), a 10 μm × 1 mm rectangular cross-section of single-crystal silicon was studied as shown in Figure 3, where 10 μm stands for an area large enough for the study of micro scale single crack, and 1 mm is the total target depth. A micro scale notch with 1–4 μm lengths, 0.2 μm height, and 2–26 μm depths on the upper left corner was preset in the square. The notch stands for the potential crack source, which probably evolved from the original defect through defect generation, migration, and nucleation (Masters & Gorey 1978; Gao *et al.*, 2014). According to (Bailey & Sethna 2003), the crack opening angle can significantly affect the value of the critical stress intensity factor. For this reason, a U -type notch was used rather than a V -type one.

In this work, as thermal stress induced by CPF is the applied load, the thermal conduction process should be taken into consideration. Thus, Fourier heat conduction equation was adopted as the governing equation:

$$\rho C_v \frac{\partial T}{\partial t} = \lambda \nabla^2 T + P \quad (1)$$

where ρ , C_v , and λ are the mass density, specific heat, and thermal conductivity of the target, respectively, and all of them are temperature-dependent parameters. Worth to mention, based on our evaluation, the melt layer depth is within half micrometer, which is also demonstrated in (Dojčinović *et al.*, 2010). Therefore, the phase change process was not taken into account in this work.

Based on our previous work (Yu *et al.*, 2015), the external heat source term $P(x, y, t)$ induced by CPF can be defined as:

$$P(x, y, t) = U(x) \cdot d(y) \cdot g(t) \quad (2)$$

Here $P(x, y, t)$ is the power density distribution on the target induced by IPIB. $U(x)$ is the cross-sectional energy distribution function. As the studied sample size in this work is 10 μm much smaller than the beam spot (around one centimeter), so $U(x)$ can be approximately replaced by a constant; $d(y)$ shown in Figure 4a is the dimensionless depth-normalized energy loss distribution over the depth y , which can be readily obtained by simulating the penetration of 1.25 keV protons efficiently accelerated by inter-electrode voltage with Monte Carlo software SRIM (Ziegler *et al.*, 2010). When considering the power density in material, it is assumed that the deposited energy from CPF is mainly contributed by positive ions when taking the mass difference and shot range difference between ions and electrons into consideration. Multiple trials of simulation have been carried out with various shapes of $d(y)$, like rectangular or triangular distribution within a depth range of 20–500 nm, which showed that no significant difference was generated as long as the energy density value was fixed; $g(t)$ shown in Figure 4b is the dimensionless time-normalized power density evolution function, which can be calculated with the current waveform obtained in (Dojčinović *et al.*, 2007a).

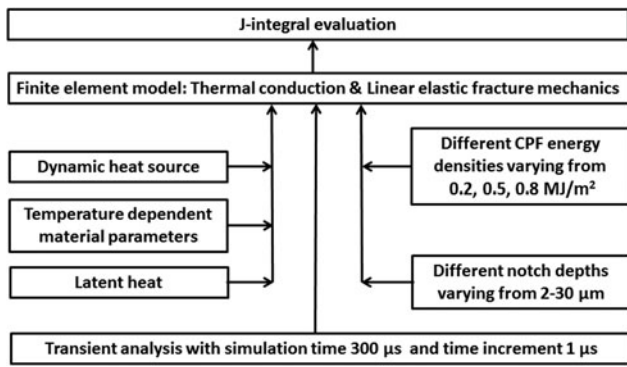


Fig. 2. The schematic diagram of the analytical model.

For initial condition, we took:

$$T(x, y, 0) = T_0 \tag{3}$$

here T_0 is room temperature 298 K.

For boundary condition, Stefan–Boltzmann boundary condition was taken for the upper surface to evaluate the energy loss by infrared radiation:

$$j = \epsilon_E \sigma_S (T^4 - T_0^4) \tag{4}$$

where j is the surface-to-ambient radiative heat flux, ϵ_E is the emissivity, which here takes 0.5 for silicon, and σ_S is the Stefan–Boltzmann constant; adiabatic boundary was adopted for the rest boundaries. In addition, as the air pressure in the vacuum chamber is quite low, convective thermal transfer is not taken into consideration, either.

Up to now, the temperature evolution over the studying area can already be obtained. In order to analyze the stress and strain configuration after CPF action, elastic linear mechanics is considered for silicon as well.

As an expression of Newton’s second law, the material’s motion equation was adopted to describe the thermodynamic process:

$$\nabla \cdot \sigma = \rho \frac{\partial^2 \mathbf{u}}{\partial t^2} \tag{5}$$

where σ , ρ , \mathbf{u} stand for Cauchy stress tensor, mass density, and displacement vector, respectively.

The relationship between strain and displacement is defined with infinitesimal strain theory:

$$\epsilon = \frac{1}{2} [\nabla \mathbf{u} + (\nabla \mathbf{u})^T] \tag{6}$$

where ϵ is the infinitesimal strain tensor, while $(\nabla \mathbf{u})^T$ is a transpose of $\nabla \mathbf{u}$.

The general equation for Hooke’s law to describe the elastic material behavior:

$$\sigma = \mathbf{D} \epsilon_{el} = \mathbf{D} (\epsilon - \epsilon_{th}) \tag{7}$$

where \mathbf{D} is the elasticity matrix, ϵ_{el} and ϵ_{th} are the elastic strain and thermal strain, respectively.

Zero displacement boundary conditions are set for all the boundaries except the upper surface, which is unrestricted in this model.

To combine the thermal conduction model and linear elastic mechanics model, temperature distribution was connected to thermal strain with:

$$\epsilon_{th} = \alpha (T - T_0) \tag{8}$$

where α is the temperature-dependent coefficient of thermal expansion. The above equations were solved by Comsol Multiphysics, a finite element method (FEM) tool. Time step for the solution is 1 μ s and the whole study duration is 300 μ s.

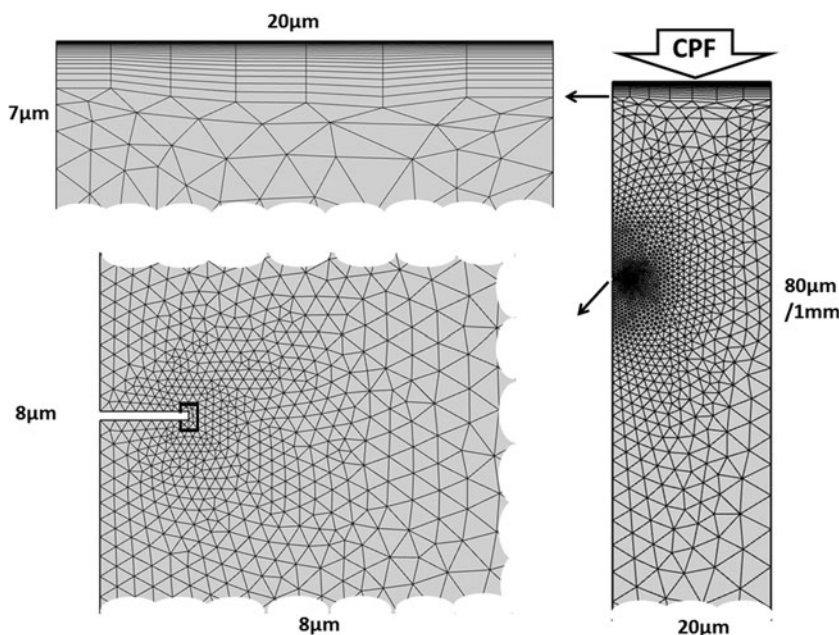


Fig. 3. Meshed two-dimensional cross-section of single-crystal silicon irradiated by CPF with a crack tip surrounded by a J -integral path.

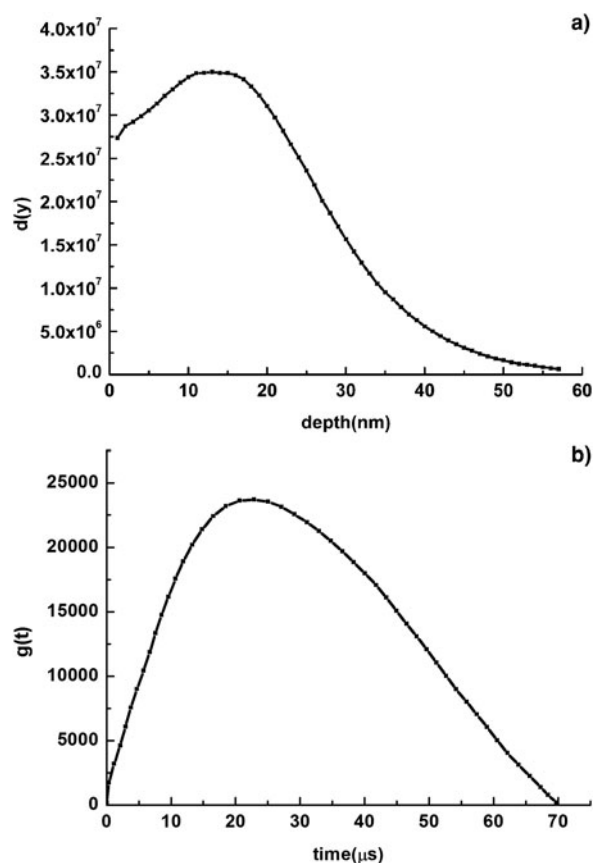


Fig. 4. (a) Depth-normalized energy loss per unit length in material surface for ions in CPF; (b) time-normalized energy distribution of CPF during the first 70 μ s.

J Integral analysis

In scientific research, there was a strong desire for natural phenomena at a fundamental level. To explain fracture physically, the famous Griffith theory (Griffith 1921) treats critical fracture as an equilibrium state when the strain energy loss can be equated to the newly generated surface energy due to the crack growth of an infinitesimal length. Proposed by Eshelby (Eshelby 1999) and Rice (Rice 1968), J integral is a path-independent parameter in a line integral form, which has been widely used due to its attractive features.

In this work, since now the dynamic evolution of the stress and strain field around the crack tip can already be calculated quantitatively, a valid method has to be employed to predict the crack growth. As an effective bridge to connect the strain field around the crack tip to the strain energy release rate, J integral becomes a promising candidate. To be specific, J integral is a two-dimensional line integral along Γ , a counterclockwise contour surrounding the crack tip shown in Figure 3. It is defined as:

$$J = \int_{\Gamma} (W dy - \mathbf{T}_i \frac{\partial u_i}{\partial x} ds) \quad (9)$$

where W is the strain energy per unit volume subjected to arbitrary stresses:

$$W = \frac{1}{2} (\sigma_x \cdot \varepsilon_x + \sigma_y \cdot \varepsilon_y + 2 \cdot \sigma_{xy} \cdot \varepsilon_{xy}) \quad (10)$$

And \mathbf{T} is the traction vector defined according to the outward normal unit vector \mathbf{n} along Γ :

$$\mathbf{T}_i = \sigma_{ij} \cdot \mathbf{n}_j \quad (11)$$

With the J integral parameter, K_I factor which can be obtained if treating silicon as linear elastic:

$$K_I = \sqrt{\frac{J \cdot E}{1 - \nu^2}} \quad (12)$$

where E is the Young's modulus and ν is the Poisson's ratio. K factor can be applied as a criterion if comparing it with the critical stress intensity factor K_{IC} for different materials. In other words, in a dynamic loading case, one can obtain the critical J parameter J_C for a specific material, and compare the dynamic J parameter with J_C as a criterion to judge if the crack can initiate or not. All the parameters mentioned above correspond to single-crystal silicon (100). Worth to mention, different crystallographic directions of silicon wafer have different critical stress intensities (Johansson *et al.*, 1989). Critical stress intensity for silicon (100) in our work was utilized to obtain critical J_C in accordance with the actual wafer used in (Dojčinović *et al.*, 2010).

FEM simulation results

As reported in (Dojčinović *et al.*, 2010) that two kinds of fractures are formed on single-crystal silicon after CPF action: one is the waffle-like surface fracture and the other is the interlaminar fracture, which finally leads to exfoliation. According to the previous work (Kovivchak *et al.*, 2012), the former fracture develops along the cleavage plane due to fast quenching process. Its formation mechanism can be comparable to that of mud-crack (Shorlin *et al.*, 2000). Due to the fast temperature rise induced by CPF within the first hundred μ s in time and several μ m in depth, the material surface was rapidly expanded (Astashynski *et al.*, 2006). Closely after that, the surface temperature decreases sharply and inevitably leads to shrinkage. In such a rapid stress load, the material cannot behave with only elastic deformation. Therefore, fracture is launched to release the energy, and naturally it develops along the cleavage plane where the minimum binding energy exists. Thus, the waffle-like surface fracture is achieved.

When it comes to the interlaminar fracture, the waffle-like fracture has made the silicon surface into separated blocks, and the interlaminar fracture is driven to initiate in mode I by thermal loading. In this way, the exfoliation region is generated with a depth around 10 μ m. The exfoliated shape is restricted into square for silicon (100) or rhombus with 60 and 120° corners for silicon (111). It can be readily calculated by SRIM that the ion range for the protons in CPF in this case is much smaller than 1 μ m. So it can be deduced that the interlaminar crack develops in deeper depth than ion range. Because of the pressure gradient induced by shock-wave effect, the modified layer of the surface depth is much larger than the CPF ion range. In this case, to figure out the exfoliation mechanism, and thus optimize the CPF parameter in future industrial application, it becomes important to develop a model which enables us to evaluate the modified layer status and forecast the crack behavior after CPF action.

By simulation, the typical distributions of temperature and stress are illustrated in Figure 5. The existence of the preset notch breaks the symmetry of distribution, and makes it

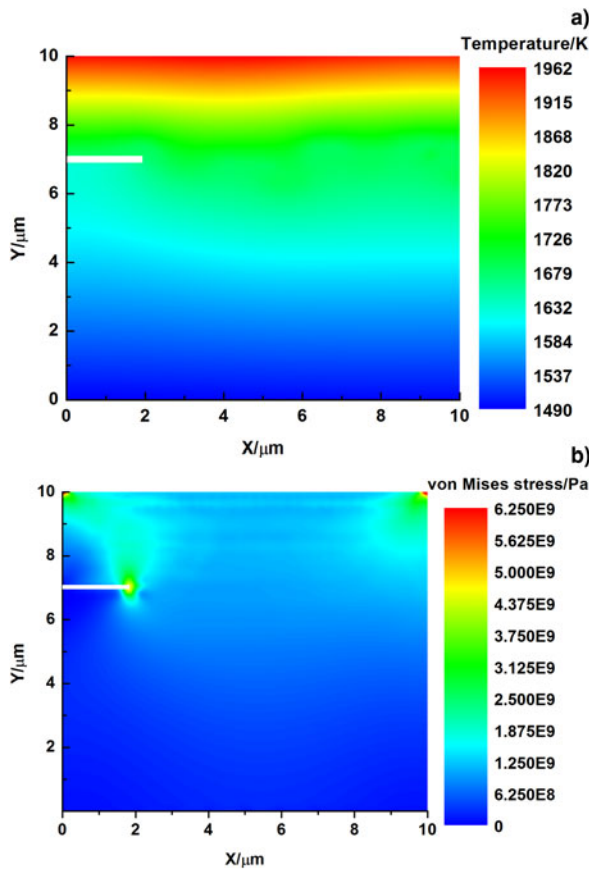


Fig. 5. The distribution of (a) temperature and (b) stress field at 15 μs induced by CPF with cross-sectional energy density of 0.5 MJ/m^2 in single-crystal silicon.

non-uniform at the same depth. A large gradient of temperature and stress in the surface layer can still easily be figured out. As indicated in (Uglov *et al.*, 2010), GPa level shock wave will be generated under CPF action. The maximum value in stress distribution in Figure 5b can also arrive at this level. But we can see the maximum is located at geometric corners where stress is concentrated. From the distribution, one can hardly figure out whether the fracture can initiate from the notch or not. In this case, numerical evaluation will be more convincing than qualitative analysis in the fracture initiation issue. That is why J integral should be applied next.

Model validity

One big issue of the model applicability for CPF thermal load is to verify its validity. The first concern is that CPF action is a dynamic thermal loading process, and the path-independent J integral may not work. As shown in Figure 6a, the trial was carried out with four different paths around the crack tip. The paths 1–4 are in square shape with side lengths of 0.5, 1.0, 1.5, and 2.0 μm , respectively. One can see no big difference exists in the evaluation results between these paths. It can conclude that the choice of integral path will not bring uncertainty to the result.

Another concern is that whether the choice of the dimension of the notch will affect the evaluation result. The defect size in single-crystal silicon varies from several nm to hundreds of nm. As J integral can slightly increase with notch height, the notch height is fixed in this work at 0.2 μm according to the maximum

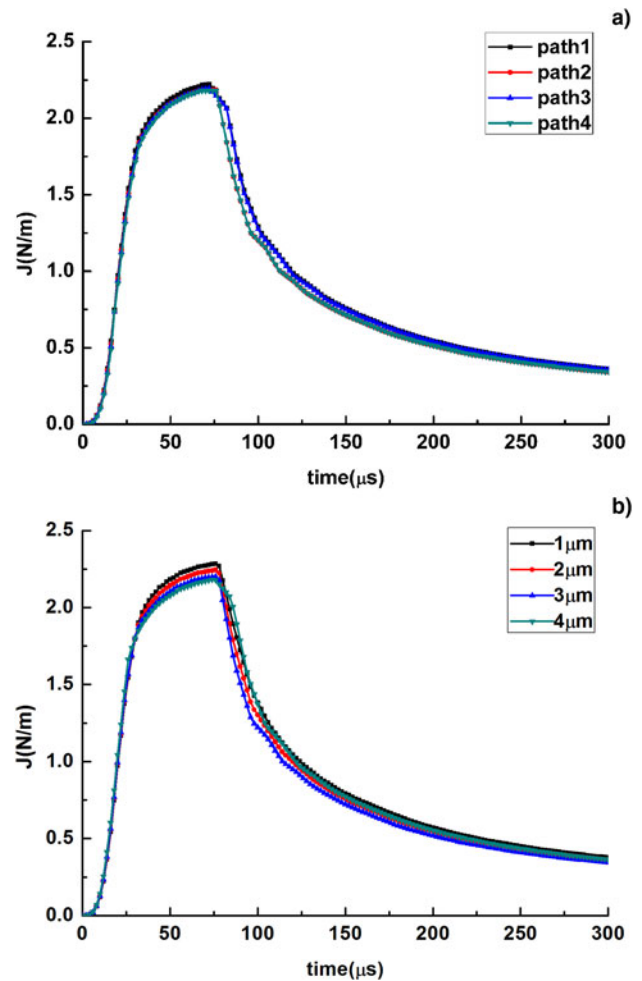


Fig. 6. J integral value for 0.2 MJ/m^2 CPF and 6 μm depth notch at different (a) paths and (b) notch lengths.

defect size reported in (Vanhellemont *et al.*, 1997). After CPF action, the defects may generate, migrate, and nucleate as has been stated above. Especially under such powerful shock wave, due to the defect connection mechanism (Gnyusov *et al.*, 2016), the crack source may become longer than original defect size. Figure 6b presents different results with various notch lengths, from which one can conclude that the choice of notch length will make limited difference in the evaluation.

Evaluation results and discussion

To analyze the stress distribution around the crack tip after CPF, thermal conduction model and linear elastic mechanics model are combined. After obtaining the temperature and stress distribution, J integral now should be applied to estimate the energy release rate around the crack tip. The J parameter can be obtained as a criterion of crack growth by comparing with critical value J_C . Worth to mention, the critical fracture toughness K_{IC} , which can be readily transformed to J_C for micro scale single-crystal silicon has been intensively studied with experiment (Fitzgerald *et al.*, 2000; Sundararajan & Bhushan 2002) or molecular dynamic simulation (Bailey & Sethna 2003). In this work, a fixed value 5.1 N/m specifically for Si (100) (Johansson *et al.*, 1989) is taken as shown in Figure 7.

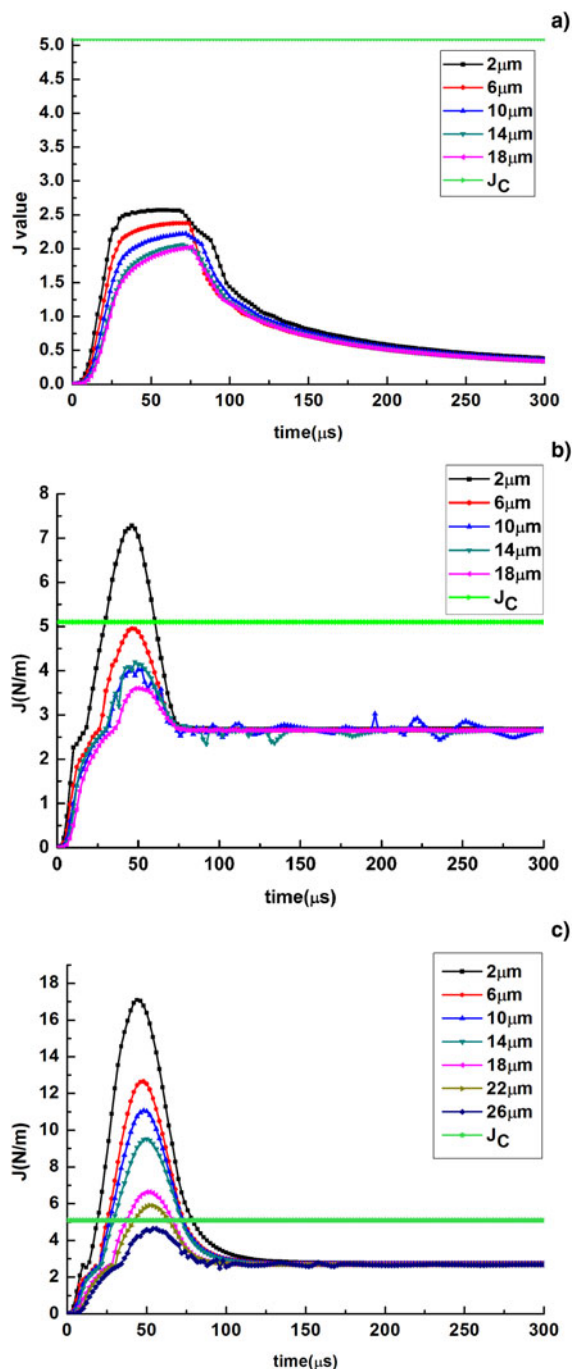


Fig. 7. The evolution of J integral parameter during the first 300 μs for mode I interlaminar fracture generated at different depths under the action of CPF with energy density at: (a) 0.2; (b) 0.5; (c) 0.8 MJ/m^2 .

When considering the effect of crack depth, it is demonstrated in Figure 7 that with a specific energy density and larger depth, J value decreases and the peak value comes later. The latter represents the peak of shock wave, and it is easy to understand that shock wave attenuates during propagating and deeper crack interacts with shock wave later.

When it now comes to the energy density, the situation varies. For low-energy density in Figure 7a, the J integral for the surface layer is much smaller than the critical value, which indicates that no interlaminar fracture can initiate at this case. When energy

density comes to 0.5 MJ/m^2 as shown in Figure 7b, it seems possible for interlaminar fracture to develop within a very shallow layer. However, one cannot easily conclude that exfoliation must occur within these several μm . That is because exfoliation needs a suitable crack source, whose existence depends on the defect distribution status. For CPF with 0.8 MJ/m^2 energy density as shown in Figure 7c, the depth range for interlaminar fracture development is within 22 μm . In this case, considering the defect density in single-crystal silicon, there will probably be suitable crack source, which can finally lead to interlaminar fracture.

Based on the above results, it becomes easy to explain the experimental result that the exfoliation only occurs in the central part of the target (Dojčinović *et al.*, 2007b; Dojčinović *et al.*, 2010). It is claimed that with conducted calorimetric measurement, the power density of typical CPF ranges from 0.5×10^5 to $3 \times 10^5 \text{ W}/\text{cm}^2$ in 120 μs discharge duration depending on the sample location (Uglov *et al.*, 2002). In the experiment, the sample was placed 5 cm away from the cathode (Dojčinović *et al.*, 2010). That is to say the averaged CPF energy density deposited in the 1 cm^2 target material is around 0.36 MJ/m^2 . According to the high-speed camera frames in, it can be deduced that CPF cross-sectional energy distribution is non-uniform with rotational axisymmetry. The CPF size is 1 cm in diameter, which indicates that the outermost energy density on the silicon sample is closed to zero (Dojčinović *et al.*, 2007a, b). No matter it is Gaussian or cone-shaped distribution, the maximum energy density in the center is roughly estimated to be around 0.72 MJ/m^2 . According to the statement in (Dojčinović *et al.*, 2007a, b), the energy density in the peripheral part without surface fracture is 10 J/cm^2 , that is, 0.1 MJ/m^2 . To sum up, the critical energy density for the initiation of surface interlaminar fracture should be located within the range of 0.1–0.72 MJ/m^2 , which is consistent with the simulation result. Future measurement of more accurate value for the critical energy density depends on the development of CPF diagnostic technique with higher spatial resolution like infrared camera technique, which has already been successfully applied for other transient thermal load (Yu *et al.*, 2015).

Worth to mention, to evaluate the possibility of the interlaminar crack growth, not only silicon, two widely used metals are studied with this model as well. Based on the material book (Vable 2012), K_{IC} of steel alloy and aluminum alloy are 150 and 37 $\text{MPa}\sqrt{\text{m}}$, respectively. Both of them are far beyond the calculated maximum K_{I} value by this model. However, here it is assumed that materials are single crystal. For engineering materials, more aspects should be taken into consideration for this model.

Conclusion

To understand the interlaminar fracture produced on single-crystal silicon under the action of CPF, a FEM model combining thermal conduction and linear elastic mechanics with J integral theory was built. The dynamic temperature and stress distributions were obtained. The J integral model was proved valid by trials with different integral paths and crack source lengths.

With this model, it can be concluded that:

- (1) For CPF with a specific energy density, it is more difficult for deeper cracks to develop.
- (2) There is a minimum value of energy density for CPF to generate interlaminar fracture and exfoliation. For single-crystal silicon (100), it is around 0.5 MJ/m^2 .

- (3) With higher energy density of CPF, larger range of depth is possible for interlaminar fracture generation.

The model will be beneficial for the choice of modified target and optimization of IPIB parameter, and it has a potential application in the intense pulsed ion/electron beam or other thermal processing techniques for material surface as well.

Acknowledgments. This work was supported by the National Natural Science Foundation of China (Grant No. 11175012), China Postdoctoral Science Foundation (Grant No. 2016M600897), and Magnetic Confinement Fusion Program (Grant No. 2013GB109004). In addition, the authors express their sincere gratitude to Professor Ivan Dojčinović from the University of Belgrade, Serbia, for his permission to use the experimental figure in his published paper.

References

- Astashynski VM, Ananin SI, Askerko VV, Kostyukevich EA, Kuzmitski AM, Uglov VV, Anishchik VM, Astashynski VV, Kvasov NT and Danilyuk AL (2004) Materials surface modification using quasi-stationary plasma accelerators. *Surface and Coatings Technology* **181**, 392–395.
- Astashynski VM, Ananin SI, Emelyanenko AS, Kostyukevich EA, Kuzmitski AM, Zhvavy SP and Uglov VV (2006) Bulk periodic structures formation on monocrystalline silicon surface under the action of compression plasma flows. *Applied Surface Science* **253**(4), 1866–1872.
- Bailey NP and Sethna JP (2003) Macroscopic measure of the cohesive length scale: Fracture of notched single-crystal silicon. *Physical Review B* **68**(20), 205204-1-8.
- Danilewsky A, Wittge J, Kiefl K, Allen D, McNally P, Garagorri J, Elizalde MR, Baumbach T and Tanner BK (2013) Crack propagation and fracture in silicon wafers under thermal stress. *Journal of Applied Crystallography* **46**, 849–855.
- Dojčinović IP, Kuraica MM, Obradović BM, Cvetanović N and Purić J (2007a) Optimization of plasma flow parameters of the magnetoplasma compressor. *Plasma Source Science Technology* **16**, 72–79.
- Dojčinović IP, Kuraica MM and Purić J (2007b) Silicon single crystal surface modification by compression plasma flow action. *Publications De L'observatoire Astronomique De Beograd* **82**(82), 71–82.
- Dojčinović IP, Kuraica MM and Purić J (2010) Material surface damage by quasistationary compression plasma flow action. *Vacuum* **85**, 596–600.
- Eshelby JD (1999). *Energy Relations and the Energy-Momentum Tensor in Continuum Mechanics*. Berlin Heidelberg: Springer, pp. 82–119.
- Federici G, Andrew P, Barabaschi P, Brooks J, Doerner R, Geier A, Herrmann A, Janeschitz G, Krieger K, Kukushkin A, Loarte A, Neu R, Saibene G, Shimada M, Strohmayer G and Sugihara M (2003) Key ITER plasma edge and plasma-material interaction issues. *Journal of Nuclear Materials* **313–316**, 11–22.
- Fitzgerald AM, Dauskardt RH and Kenny TW (2000) Fracture toughness and crack growth phenomena of plasma-etched single crystal silicon. *Sensors and Actuators* **83**, 94–199.
- Gao YY, Qin Y, Dong C and Li GZ (2014) From crater eruption to surface purification of raw silicon: a treatment by pulsed electron beam. *Applied Surface Science* **311**, 413–421.
- Garkusha IE, Malykhin SV, Makhlai VA, Pugachev AT, Bazdyrieva SV and Aksenov NN (2014) Changes in the structure and substructure of tungsten during irradiation by hydrogen plasma flows at the specific energy close to the heat loads on the ITER surface. *Technical Physics* **59**(11), 1620–1625.
- Gnyusov SF, Rotshtein VP, Mayer AE, Rostov VV, Gunin AV, Khishchenko KV and Levashov PR (2016) Simulation and experimental investigation of the spall fracture of 304L stainless steel irradiated by a nano-second relativistic high-current electron beam. *International Journal of Fracture* **199**, 59–70.
- Griffith AA (1921) The phenomena of rupture and flow in solids. *Philosophical Transactions of the Royal Society of London* **221**, 163–198.
- Johansson S, Ericson F and Schweitz J (1989) Influence of surface coatings on elasticity, residual stresses, and fracture properties of silicon microelements. *Journal of Applied Physics* **65**(1), 121–128.
- Kovivchak VS, Panova TV, Krivozubov OV, Davletkil'deev NA and Knyazev EV (2012) Surface damages on single-crystal silicon during irradiation by a powerful ion beam. *Journal of Surface Investigation. X-ray, Synchrotron and Neutron Techniques* **6**(2), 244–247.
- Masters BJ and Gorey EF (1978) Proton-enhanced diffusion and vacancy migration in silicon. *Journal of Applied Physics* **49**(5), 2717–2724.
- Remnev GE, Uglov VV, Shymanski VI, Pavlova SK and Kuleshovb AK (2014) Formation of nanoscale carbon structures in the surface layer of metals under the impact of high intensity ion beam. *Applied Surface Science* **310**, 204–209.
- Rice JR (1968) A path independent integral and the approximate analysis of strain concentration by notches and cracks. *Journal of Applied Mechanics* **35**, 379–386.
- Shen J, Yu X, Zhang YY, Zhong HW, Zhang J, Qu M, Yan S, Zhang GL, Zhang XF and Le XY (2015) Novel microstructures on the surfaces of single crystal silicon irradiated by intense pulsed ion beams. *Nuclear Instruments and Methods in Physics Research Section B* **365**, 26–29.
- Shen J, Shahid I, Yu X, Zhang J, Zhong HW, Cui XJ, Liang GY, Yu X, Huang WY, Yan S, Zhang GL, Zhang XF and Le XY (2017) Fracture analysis of surface exfoliation on single crystal silicon irradiated by intense pulsed ion beam. *Nuclear Instruments and Methods in Physics Research B* **413**, 6–12.
- Shorlin KA, Bruyn JR, Graham M and Morris SW (2000) Development and geometry of isotropic and directional shrinkage-crack patterns. *Physical Review E* **61**(6), 6950–6957.
- Sundararajan S and Bhushan B (2002) Development of AFM-based techniques to measure mechanical properties of nanoscale structures. *Sensors and Actuators, A: Physical* **101**, 338–351.
- Tanaka M, Higashida K, Nakashima H, Takagi H and Fujiwara M (2006) Orientation dependence of fracture toughness measured by indentation methods and its relation to surface energy in single crystal silicon. *International Journal of Fracture* **139**, 383–394.
- Uglov VV, Anishchik VM, Astashynski VV, Astashynski VM, Ananin SI, Askerko VV, Kostyukevich EA, Kuzmitski AM, Kvasov NT and Danilyuk AL (2002) The effect of dense compression plasma flow on silicon surface morphology. *Surface and Coatings Technology* **158–159**, 273–276.
- Uglov VV, Remnev GE, Kuleshov AK, Astashynski VM and Saltymakov MS (2010) Formation of hardened layer in WC–TiC–Co alloy by treatment of high intensity pulse ion beam and compression plasma flows. *Surface and Coatings Technology* **204**, 1952–1956.
- Vable M (2012) *Mechanical Properties of Materials*. Springer, vol. **190**, p. 645.
- Vanhellemont J, Senkader S, Kissinger G, Higgs V, Trauwaert MA, Gräf D, Lambert U and Wagner P (1997) Measurement, modelling and simulation of defects in as-grown Czochralski silicon. *Journal of Crystal Growth* **180**, 353–362.
- Yu X, Shen J, Qu M, Liu W, Zhong HW, Zhang J, Zhang YY, Yan S, Zhang GL, Zhang XF and Le XY (2015) Characterization and analysis of infrared imaging diagnostics for intense pulsed ion and electron beams. *Vacuum* **113**, 36–42.
- Zhao WJ, Remnev GE, Yan S, Opekounov MS, Le XY, Matvienko VM, Han BX, Xue JM and Wang YG (2000) Intense pulsed ion beam sources for industrial applications. *Review of Scientific Instruments* **71**(2), 1045–1048.
- Ziegler JF, Ziegler MD and Biersack JP (2010) SRIM – the stopping and range of ions in matter (2010). *Nuclear Instruments and Methods in Physics Research Section B* **268**, 1818–1823.